CrossMark

Efficient removal of uranium(VI) from aqueous medium using ceria nanocrystals: an adsorption behavioural study

Kuntaiah Kuncham[1] · Sajitha Nair[1] · Smeer Durani[1] · Roopa Bose[1]

Abstract Ceria nanocrystals were synthesized by template free and cost effective method for highly efficient adsorption of U(VI) from aqueous solutions. In this study we investigated the factors influencing the adsorption behavior of U(VI) onto the ceria nanocrystals like pH, dosage, time of contact and initial metal ion concentration. The mechanism of adsorption was elucidated based on the isothermal and kinetic studies. A monolayer surface adsorption of uranyl ions onto the ceria nanocrystals with an adsorption capacity of 270 mg/g involving adsorptive pore filling and electrostatic interactions was indicated. The ceria nanocrystals could be regenerated and reused without significant reduction of adsorption capacities.

Keywords Ceria nanocrystals · Uranium(VI) · Isotherms · Kinetics · Adsorption capacity

Introduction

Environmental pollution crisis due to the industrial revolution has become one of the most formidable challenges gaping at the human society at large. The intense development in the field of nanoscience and nanotechnology is significant and a mammoth step forward in the field of removal of toxic and heavy metal ion contaminants like Cr(VI), As(V), Pb(II), Zn(II), Cd(II) and U(VI) from various industrial effluents including nuclear industry as well as potable and ground water. They exhibit features superior to bulk materials for adsorption primarily due to properties like quantum size effect contributing to large specific surface area and enhanced density of surface defects promoting large number of active sites for various applications [1, 2]. So far, various nanosized materials have been reported for the environmental detoxification which includes iron oxide [3], magnesium oxide, mixed valence manganese oxides, aluminium/titanium/zinc oxides [4], nanosized cerium oxide [5], etc. Particularly detailed studies of U(VI) adsorption on various nanoscale adsorbents like hollow SiO_2 microspheres functionalized with amidoxime [6], nanoscale zero valent iron on activated charcoal [7], diamine functionalized hollow silica microspheres [8], hydrous TiO_2 [9] and graphene oxide [10] have been reported extensively.

The emphasis in the field of industrial application of nanosized materials in environmental remediation is on the development of cost effective, simple and rapid methods for designing novel non-toxic nanosized materials which can efficiently and selectively remove various concomitants present in the environment and also can be easily recovered and reused for several cycles. Amongst various nanosized materials used, rare earth oxides like ceria [11] have been a significant contributor with a difference. Properties of ceria vary significantly with different morphologies, sizes, shapes, surface areas and exposed crystal phases which are further enhanced and newer properties introduced when reduced particularly to nano size [12]. The distinctive feature of CeO_2 is the easily accessible oxidation states of cerium ions (Ce(III)/Ce(IV)) accompanied by generation of oxygen vacancies [13]. Based on this inherent property cerium oxide nanoparticles are

✉ Roopa Bose
   roopaboseamd@gmail.com

1 Chemistry Laboratory, Department of Atomic Energy, Atomic Minerals Directorate for Exploration and Research, Nagarbhavi, Bangalore 560072, India

efficient free radical scavengers and are considered as a potent therapeutic option for the treatment of ROS mediated disorders like neurodegenerative disorders, retinal disorders, cancer and can also act as a potent drug delivery agent [14]. The 3D flower like ceria nanocomposite structures synthesized via micelle supported route has been used for remediation of industrial effluents for As(V) and Cr(VI) [11]. Similarly Peng and coworkers [15, 16] showed that CeO_2-CNT nano materials were effective adsorbents for As(V) and Cr(VI). Ceria hollow nanospheres produced by template free microwave assisted hydrothermal method showed adsorption capacity of 22.4 mg/g for As(V) and 15.4 mg/g for Cr(VI) [17]. Chemically synthesized CeO_2 powder has been used for the adsorption of zinc and cadmium ions from aqueous waste solutions [18]. Ceria hollow nano spheres, flower like ceria and commercial bulk ceria with BET surface areas of 72, 34.1 and 2 (m^2/g), respectively, exhibited maximum removal capacity of As(V) and Cr(VI) varying between 0.3 to 22.4 mg/g for As(V) and 0.37 to 15.4 mg/g for Cr(VI) respectively [17]. Though detailed literature survey as mentioned above indicates that there have been several adsorption and decontamination studies with respect to uranium and other toxic elements in presence of a variety of nano adsorbents but no specific and elaborate adsorption studies with ceria nanocrystals of the chemically toxic radionuclide uranium in aqueous medium has been reported so far.

Herein, we report a template free, low cost and eco-friendly method of preparation of ceria nanocrystals with a BET surface area of 41 m^2/g which accommodates very efficiently the uranyl ion yielding a Q_{max} (maximum adsorption capacity) of 270 mg/g. The large surface area achieved due to the scaling down to nanosize and the resulting efficient mass transfer of the metal nuclei on to the surface/subsurface active sites, has resulted into a very efficient uranium remediation methodology for contaminated water like mine effluents. This optimized method can also be applied for the preconcentration of uranium in sea water like environment. This study includes a detailed understanding of the equilibrium adsorption mechanism of U(VI) ions on ceria nanocrystals by investigating the influence of different experimental parameters affecting the adsorption process and capacity of the synthesized adsorbent. Kinetic and isothermal modeling of the system has been attempted in detail for a better understanding of the equilibrium mechanism.

Experimental

Materials

All chemicals were of AnalR grade and were used without any further purification. $UO_2(NO_3)_2 \cdot 6H_2O$ (ACS grade),

Merck Germany was used to prepare U(VI) ion stock solution. 10% HNO_3 and aq NH_4OH were used to adjust pH of the working solution. The concentration of the metal ion in the supernatant after adsorption was determined using Inductively Coupled Plasma Atomic Emission Spectroscopy [Jobin–Yvon 2000(2)] and LED flourimeter (Quantalase). Deionsed water was used for all experiments obtained from MilliQ (Millipore Corporation) water purification system. Some of the anions and the cations in real samples (Na, K) were measured using Flame Photometer (Elico India make), Ca and Mg by titrimetry, sulphate by turbidimetry and fluoride using Ion selective electrode (Extec India make), respectively. The pH of all solutions was measured by pH meter (Elico India make).

Synthesis of ceria nanocrystals

Nanosized cerium oxide was prepared [19] by adopting a co-precipitation method using cerium nitrate [$Ce(NO_3)_3 \cdot 6H_2O$ 99.9% Aldrich] as the precursor. The required amount of precursor was dissolved in double distilled water under mild stirring condition. Hydrolysis of metal salt to hydroxides was carried out by drop wise addition of aqueous ammonia solution until pH of the solution reached 9.5. The obtained light yellow colored precipitate was decanted, filtered and washed with double distilled water multiple times to remove the weakly adhered nitrate ions from the surface. Further, it was oven dried at 393 K for 12 h. The oven dried sample was further crushed using an agate mortar and calcined at 773 K for 5 h.

Characterization of ceria nanocrystals

The powder X-ray diffraction patterns were recorded on a Rigaku diffractometer using Cu Kἀ radiation (0.15418 nm) radiation source and a scintillation counter detector (SCD). The scattered intensity data were collected from 2θ values of 2°–80° by scanning at 0.02° steps with a counting time of 2.4 s at each step. The XRD phases present in the sample was identified with the help of Powder Diffraction File-International Center for Diffraction Data (PDF-ICDD). The average crystallite size (D) of the sample was determined with the help of Scherrer equation from line broadening which was estimated by a standard cubic indexation method using the intensity of the most prominent peak (111). The Brunauer–Emmett–Teller (BET) method was utilized to calculate the specific surface areas. UV–Vis DRS measurements were performed in the range of 200–800 nm using a GBS-Cintra 10e UV–Vis NIR spectrophotometer with an integration sphere diffuse reflectance attachment. The samples under study were diluted with KBr matrix by pelletization and the data collected was referenced to a pure KBr pellet to determine the

baseline spectrum. X-ray photoelectron spectroscopy measurements were carried out on a PHI 5400 instrument with a 200 W Mg–Kἀ probe beam. SEM image was observed by a JEOL JSM 5410 scanning electron microscope, operating with an accelerating voltage of 15 kV.

Batch adsorption experiments

Batch adsorption studies were carried out in 100 mL polyethylene beakers. The stock solution of uranium of 1000 mg/L was diluted as required and pipetted following which the pH of the solution was adjusted with aqueous ammonia and 10% HNO_3 as required, maintaining a total aqueous volume of 50 mL. To this a specified weight of the absorbent was added and the beakers were placed on the magnetic stirrer with a fixed setting to achieve a constant speed of 750 rpm at room temperature for a given time interval. The adsorbent dosage and the contact time were optimized by continuous shaking on the magnetic stirrer. The adsorption process was studied as a function of pH (1–9), initial U(VI) concentration (10–50 mg/L), adsorbent dosage, aqueous volume (50–800 mL) and contact time (0–60) min. The concentration of uranium in the supernatant was measured by LED fluorimeter/ICP-AES.

The amount of U(VI) ion adsorbed onto the adsorbent Q_e (mg/g) was calculated as follows:

$$Q_e = (C_i - C_e) \times V/W \tag{1}$$

Q_e is the heavy metal ions concentration adsorbed by an adsorbent at equilibrium (mg of metal ion/g of adsorbent), C_i is the initial concentration of metal ions in the solution (mg/L), C_e is the equilibrium concentration or final concentration of metal ions in the solution (mg/L), W is the weight of the adsorbent in grams, V is the volume of aqueous solution in litres.

The percentage of adsorption is calculated using the following equation:

$$\% \text{ adsorption} = (C_i - C_e)/C_i \times 100\% \tag{2}$$

Results and discussion

Characterization of ceria nanocrystals

The powder X-ray diffraction was used for characterization of the synthesized ceria nanocrystals, XRD spectra was obtained as shown in Fig. 1. The diffraction peaks can be indexed to (111), (200), (311), (222), (400), (331), (420) and (422) crystal faces, corresponding to the face-centered cubic-phase of CeO_2 (JCPDS, Joint Committee on Powder Diffraction Standards 34–0394). The broadened diffraction
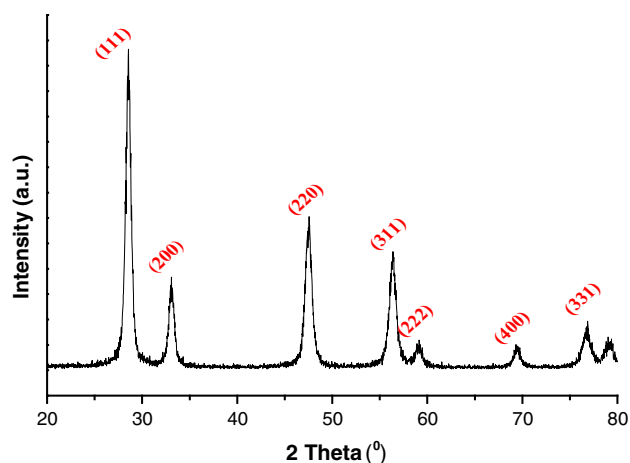

Fig. 1 Powder X–ray diffraction pattern of ceria nanocrystals calcined at 773 K temperature

peaks indicated the small size of the nanocrystals [20]. The average crystalline size of the nanocrystal was ca. 8.9 nm, as calculated from the width of diffraction peaks using the Scherrer formula. BET studies showed that the specific surface area of the nanocrystalline ceria was 41 m^2/g compared to 2 m^2/g of commercial bulk ceria [21].

SEM measurements were performed to assess the external morphologies of the ceria nanocrystal as shown in Fig. 2. As observed from the SEM images, the sample consists of typical spherical form within the narrow size range. X-ray photoelectron spectroscopic (XPS) study of Ce 3d electron core level spectra has been depicted in
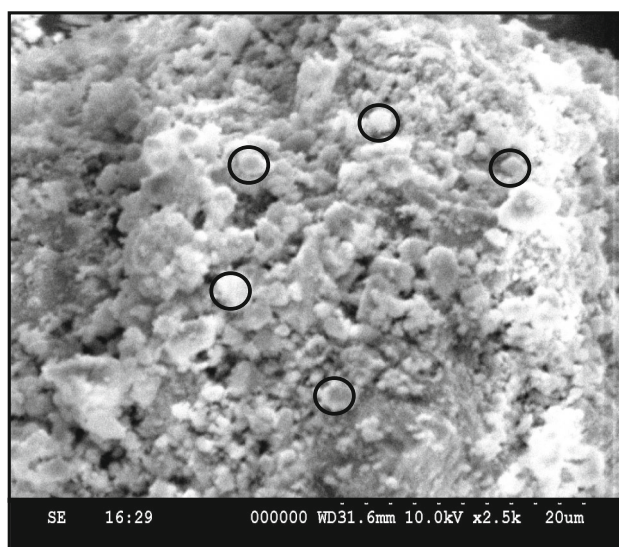

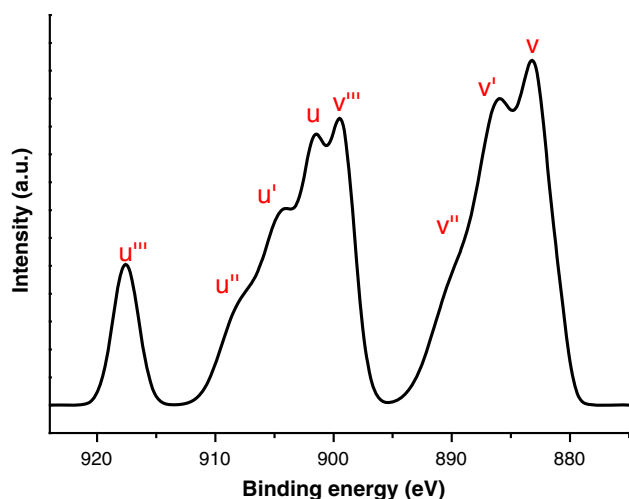**Fig. 2** SEM image of ceria nanocrystals calcined at 773 K temperature

Fig. 3 XPS spectra of ceria nanocrystals calcined at 773 K temperature
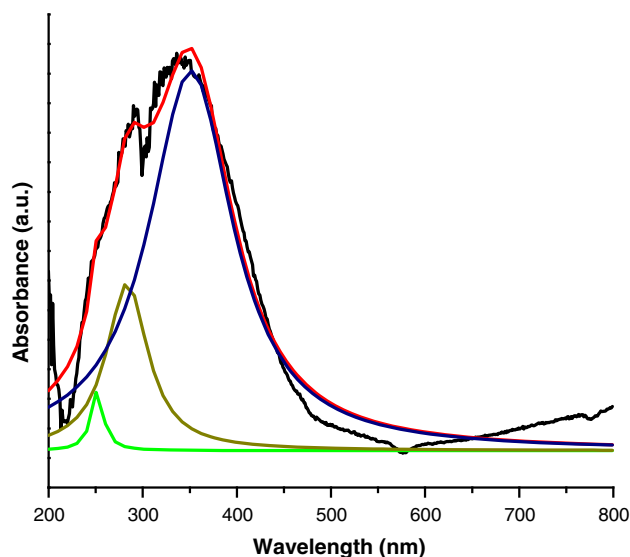

Fig. 4 UV–Vis DR spectra of ceria nanocrystals calcined at 773 K temperature

Fig. 3. These XPS studies indicated the presence of both Ce^{3+} and Ce^{4+} ions in the ceria nanocrystals.

UV–Visible DRS technique [22] provided information of the changes in bulk surface coordination and different oxidation states of ions in the adsorbent which exhibited three peaks at 255, 285 and 342 nm corresponding to $[O^{2-} \rightarrow Ce^{4+}, O^{2-} \rightarrow Ce^{3+}]$, charge transfer (CT), and interband transitions (IBT) in the wavelength range of 250–342 nm as shown in Fig. 4. Hence, reconfirming the presence of Ce^{3+} and Ce^{4+} in the crystal lattice of nanocrystalline ceria.

Effect of initial pH

The proton concentration of the aqueous phase is a significant parameter that affects the adsorption process. The species of the metal ion existing in solution and the surface charge of the adsorbent are both pH dependent [23]. Experiments were conducted in the pH range of 1–8 and the results have been depicted in Fig. 5. All metal oxides become charged by the adsorption of H$^+$ ions or OH$^-$ ions while remaining neutral at a specific pH. This pH value at which the zeta potential, the mode used to measure the surface charge, equals zero is called the isoelectric point (IP) and is used to assess adsorbent surface charge qualitatively. The published values of IP measured in ultra pure water for determination of point of zero charge of ceria nanocrystals varied from 5.8 to 7.9 [24]. The deviations from the IP values of ceria nanocrystals as reported [25] occur due to various parameters like type of impurity on the NP surface, purity of material, method of synthesis, particle size and design of titration experiment. In the present study, the IP value for ceria nanocrystal was considered to be pH ~5 which is consistent with such deviated values of the point of zero charge of ceria nanocrystals reported [26, 27]. As a result of which quantitative adsorption of the existing uranyl ion species [28] $(UO)_2)_3(OH)_5^+$, $((UO)_2)_4(OH)_7^+$, and $UO_2(OH)_2$ was observed between pH range of 5–7. The uranyl species from pH 1–4 is predominantly positively charged UO_2^{2+} ion [28] and hence the approach of this metal species towards the positively charged adsorbent surface remains unfavorable in the acidic pH range. Beyond pH 8 the trend shows gradual decrease because of the tendency of uranyl ion to remain in solution as negatively charged carbonyl species $UO_2(CO_3)_2^{2-}$, $UO_2(CO_3)_3^{4-}$ in the open system under study [29] and the approach of which is repelled by
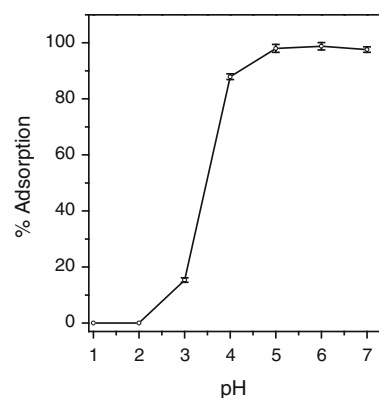

Fig. 5 pH varying, initial U(VI) concentration of 10 mg/L, total aqueous volume 50 mL and total adsorbent weight of 0.01 g

the negative surface charge of the increasingly deprotonated adsorbent surface. Thus for further studies the optimum pH chosen was 6.

Effect of adsorption dosage

Variation in total weight of adsorbent

Under the experimental conditions, initial concentration of U(VI) ions in aqueous phase being 10 mg/L at a pH of 6 and total aqueous volume of 50 mL, the effect of total weight of the adsorbent on adsorption of U(VI) ions were studied and the results have been plotted in Fig. 6. Removal efficiency of ceria nanocrystals increased with increasing adsorbent amount which is due to the large number of vacant adsorption sites and the greater available surface area favoring increased U(VI) adsorption. The quantitative removal of metal ion was achieved at 0.2 mg/mL (0.01 g in 50 mL), and hence the weight maintained for further study was the same. This effect emphasized the economic usage of the adsorbent and hence foresees the cost effective usage of this method at an industrial scale [30, 31].

Variation in total sample volume

In order to study the dependence of the adsorption process on the total aqueous volume [32], the removal ratio and the adsorption capacity were plotted with initial total volume in Fig. 7 maintaining the optimized parameters such as concentration of metal ion 10 mg/L, pH 6.0, contact time 60 min and weight of the adsorbent as 0.01 g with variation in volume of aqueous phase from 50 to 800 mL. This plot showed that there is decrease in the percentage adsorption and increase in the equilibrium adsorption capacity of the adsorbent with increase in the total volume of aqueous phase which simultaneously exhibits decrease in the adsorption dosage i.e. total weight of adsorbent per
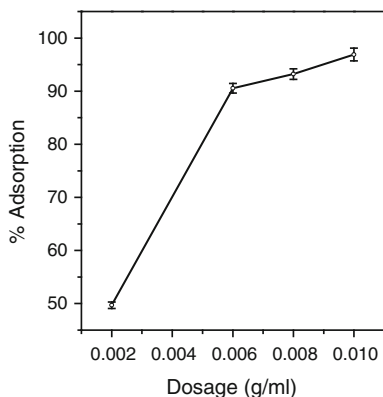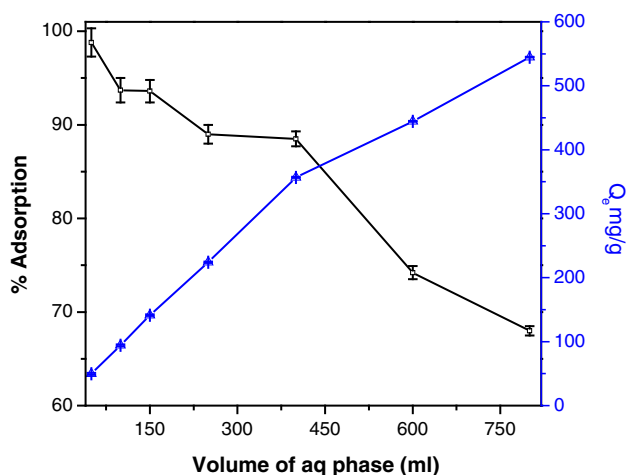

Fig. 7 Total aqueous volume: varying, initial U(VI) concentration 10 mg/L, pH 6.0, adsorbent weight 0.01 g, contact time: 60 min

unit volume. The decrease in percent adsorption as depicted in Fig. 7 is attributed to the decrease in the specific weight of the adsorbent as the aqueous phase volume increases. The increase in adsorption capacity with increase in total volume is in accordance with Eq. (1).

Effect of contact time on uranium adsorption

It is important to establish the time dependency for removal of contaminants in a solid phase adsorption process to prove the efficiency of the process. The role of time of contact on the adsorption of uranyl ion on the ceria nanocrystal was studied under the stirring conditions, for instance 750 rpm, initial uranyl ion concentration of 10 mg/L, pH of 6.0, total aqueous volume 50 mL and the total adsorbent weight of 0.01 g. The results have been plotted in Fig. 8. The removal ratio and adsorption capacity

Fig. 6 Adsorbent weight: varying, initial uranyl ion concentration of 10 mg/L, pH 6.0, total aqueous volume 50 mL
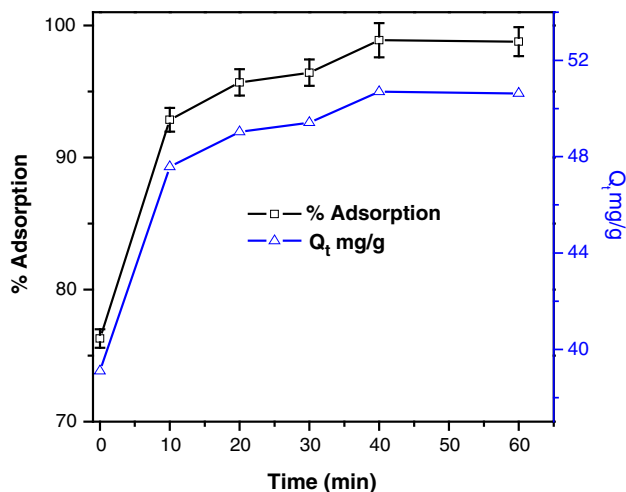

Fig. 8 Contact time: varying, initial U(VI) concentration of 10 mg/L, pH 6.0, total aqueous volume 50 mL, total adsorbent weight 0.01 g

sharply increased as the time increased initially. However the increase became gradual after a period of 10 min beyond which the adsorption gradually reached equilibrium.

Figure 8 depicts the residence time of the metal ion and defines the efficiency of the adsorbent, respectively. Initially, the rapid removal of uranyl ion was perhaps due to the vacant vast surface area of the nanocrystals and the associated available active sites responsible for the interaction with the metal ion. As the adsorption proceeded, the rate of removal of metal ion from the aqueous phase became gradual reaching a maximum within 40 min of contact time after which it remained constant as equilibrium was reached. Hence a contact time of 60 min has been maintained for all further studies.

Effect of initial uranium concentration and isotherm modeling

The relation between the initial concentration of the metal ion in the aqueous phase and the equilibrium concentration of the adsorbate on the adsorbent is very important in optimizing the adsorption process and the adsorption behavior. The adsorption capacity of the adsorbent increased with the initial metal ion concentration as depicted in Fig. 9. As uranium concentration increased in solution, a higher fraction of the ceria nanocrystal active sites were involved in the adsorption process resulting in increase in the adsorption capacity of the nanocrystals. A maximum was reached beyond which further study was restricted due to the hydrolysis of uranyl ion at the pH considered [33].

The effect of initial uranium concentration in the range of 0.5–70 mg/L on % adsorption (investigated under the optimized conditions: initial pH 6.0, contact time 60 min,
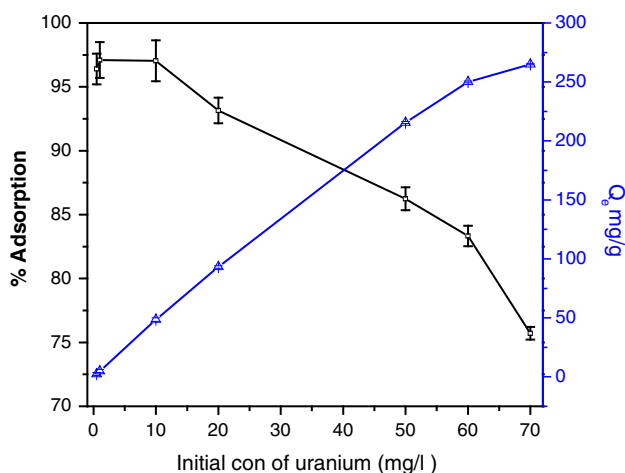

Fig. 9 Initial U(VI) concentration: varying, pH 6.0, total aqueous volume 50 mL, total adsorbent weight 0.01 g, contact time: 60 min

adsorbent dosage 0.01 g, total volume 50 mL) has also been simultaneously plotted in Fig. 9. The percent removal of the metal ion decreased with increase in the initial concentration of uranyl ion. This gradual decrease in the amount of adsorbate removed perhaps was due to the progressive increase in the occupancy of the active sites of the adsorbent.

Adsorption models

The adsorption isotherms are mathematical models significant in describing the nature of interaction between the adsorbate and adsorbent, based on a set of assumptions related to the heterogeneity/homogeneity of adsorbent, the type of available active sites and possibility of inter adsorbate interaction. Analysis of the experimentally obtained equilibrium data represented in Eqs. (4, 7) has been applied here in two isotherm models which were useful for practical design and operation of adsorption systems.

The Langmuir isotherm model [34–36] assumes monolayer coverage of the adsorption sites on to a surface containing finite number of adsorption sites of identical strategies with no trans migration of adsorbate in the plane surface. It indicates a reduction of the available interaction sites as the metal ion concentration increases. The isotherm is represented by the linear equation given below

$$Q_e = (Q_m K_L C_e)/(1 + K_L C_e) \qquad (3)$$

The linearised form being

$$C_e/Q_e = 1/K_L Q_{max} + C_e/Q_{max} \qquad (4)$$

Q_m is the maximum adsorption capacity or maximum metal uptake (in mg/g), C_e is the equilibrium concentration of uranium in mg/L remaining in aqueous solution, Q_e (mg/g) is the amount of U(VI) adsorbed on per weight unit of ceria nanocrystals after equilibrium. K_L (L/mg) is the Langmuir equilibrium constant or the rate constant which is related with the free energy change of the reaction or heat of adsorption. The linear plot of specific adsorption (C_e/Q_e) against the equilibrium concentration C_e is depicted in Fig. S1 and the parameters thus obtained have been tabulated in the corresponding Table 1.

It is observed from Table 1 that the Langmuir equation shows a significant correlation ($R^2 = 0.9897$) with the experimental data. The equilibrium adsorption capacity (Q_{max}) obtained from Langmuir model (270 mg/g) is also close to the experimentally observed saturation capacity (265 mg/g). Hence the experimental results thus obtained imply that the Langmuir adsorption model is in well correspondence with the experimental data.

The essential features of Langmuir Adsorption isotherm parameter can also be used to predict affinity between the

Table 1 Isotherm parameters of uranium adsorption by ceria nanocrystal

Model type	Q_{max} (mg/g)		K_l (L/mg)	R^2	K_f (mg/g)	n
	Theoretical	Experimental	–		–	–
Langmuir	270	265	0.5362	0.990		
Freundlich				0.964	68.97	1.33

Table 2 R_l value for uranium adsorption obtained from Langmuir equation

C_o (initial uranium concentration in mg/L)	R_l separation factor $1/(1 + K_L C_i)$
0.5	0.781
1	0.640
10	0.151
20	0.082
50	0.034
60	0.029
70	0.025

Table 3 Uranyl adsorption properties of various adsorbents

Adsorbents	Q_{max} (mg/g)	References
Tin oxide nano particles	66.67	[38]
Magnesium silicate hollow spheres	121	[23]
Graphene oxide nano sheets	97.5	[39]
Silica	14	[40]
Aminosilica	16	[40]
Benzoimidazol-2-yl-phenylphosphinic acid–silica gel	27	[40]
Zero valent iron supported on activated charcoal composite	492.6	[41]
Nano Mg(OH)$_2$	12.1	[42]
Ceria nano crystals	270	Present study

adsorbate and the adsorbant using the calculated dimensionless factor R_L tabulated in Table 2 called separation factor or equilibrium parameter and expressed as

$$R_L = 1/(1 + K_L C_i) \tag{5}$$

If $R_L = 0$ isotherm is irreversible, linear if $R_L = 1$, unfavourable if $R_L > 1$ or favourable if $0 < R_L < 1$

R_L values calculated for all the initial uranium concentrations with the obtained K_L value of 0.5362 (L/mg) lie within $0 < R_L < 1$ [37] emphasizing that ceria nanocrystal is a favorable adsorbent for uranium adsorption on energetically identical sites within the ceria nano crystal moiety. The adsorption capacities of different adsorbents have been listed in Table 3 [23, 38–42] for comparison. The maximum adsorption capacity for uranyl ions of the as-prepared adsorbent is higher than most of the other listed adsorbents.

The Freundlich isotherm assumes a heterogeneous surface with a nonuniform distribution of heat of adsorption over the surface. Therefore, it describes an energetically heterogeneous surface on which the adsorbed molecules are interactive. The isotherm is represented by the equation [43, 44]

$$Q_e = K_f \times C_e^{1/n} \tag{6}$$

The logarithmic equation being:

$$\text{Log } Q_e = \text{Log } K_f + 1/n \times 1/2.303 \text{Log } C_e \tag{7}$$

where K_f is the Freundlich constant indicating adsorption capacity and n is the adsorption intensity.

The ability of the Freundlich model to fit the experimental data was examined by plots of Log Q_e vs. Log C_e as shown in Fig. S2 on the basis of the linear form of the Eq. 7. The K_f and the n values were obtained from the intercept and the slope respectively and tabulated in Table 1. n value indicates degree of non linearity between aqueous metal ion concentration and adsorption as follows: if $n = 1$, then adsorption is linier, if $n < 1$, then adsorption is a chemical process, if $n > 1$ then adsorption is a physical process. The value of n as tabulated in Table 1 is 1.33 which is indicative of the adsorption in this study being a physical phenomenon [45]. From the data in Table 1 values

of $1/n = 0.7533$ and $n = 1.33$, indicate that the sorption of UO_2^{2+} onto ceria nano crystals is favourable and R^2 value is 0.964 [46]. Hence the sorption data fitted into Langmuir and Freundlich isotherm models out of which Langmuir isotherm model was found to have the highest regression value (R^2), therefore the best fit.

Adsorption kinetics

The kinetics of adsorption describes the rate at which the metal ion is adsorbed on the adsorbant which in turn controls the equilibrium time and influences the adsorption mechanism. The three typical processes taking place at the solid liquid interface are external diffusion including bulk and film diffusion, intraparticular diffusion and surface interaction. Agitation at the rate of more than 400 rmp negates the effect of external diffusion. The uptake kinetics has been analyzed by various kinetic models like the pseudo first order, pseudo second order kinetics and intraparticle diffusion. The kinetics studies of uranyl adsorption were carried out by batch adsorptions that formerly were used to determine optimum condition of contact time.

Pseudo first order kinetic model can be expressed by the equation

$$\text{Log}(Q_e - Q_t) = Log Q_e - K_1 t/2.303 \tag{8}$$

where Q_e and Q_t (mg/g) are the concentration of uranium adsorbed at equilibrium and at time t, K_1 (h^{-1}) is the pseudo first order rate constant [47].

The model parameters Q_e and K_1 were obtained from the linear plot of Log ($Q_e - Q_t$) against time (Fig. S3) have been tabulated in Table 4.

Pseudo second order kinetics can be expressed as

$$t/Q_t = 1/K_2 Q_e^2 + t/Q_e \tag{9}$$

K_2 is the rate constant (g/mg/h) of this model. The equilibrium adsorption capacity Q_e and the second order rate constant K_2 were obtained from the plot of t/Q_t against t [45] as depicted in Fig. S4.

Intraparticle diffusion can be expressed as

$$Q_t = K_{ip}(t)^{1/2} \tag{10}$$

K_{ip} is the intraparticle diffusion coefficient and the model parameters were obtained from the linear plot of Q_t versus $(t)^{1/2}$ as plotted in Fig. S5. The value of rate constants and correlation coefficients for each model are shown in Table 4. For the ceria nano crystal as depicted in Table 4 according to the correlation coefficients (R^2) the pseudo second order equation with a value of 0.9997 fits the experimental kinetic data better than the pseudo first order equation ($R^2 = 0.8813$) and the intraparticular diffusion model ($R^2 = 0.8664$). In addition, the comparison made between the experimental adsorption capacity (Q_e experimental) value and the calculated adsorption capacity (Q_e) values show that the calculated Q_e value of 51.02 obtained from the pseudo second order kinetic model is in good agreement with the empirically obtained Q_e value of 50.695, when compared with the value obtained from the pseudo first order kinetic model of 12.68. The high correlation coefficient value for the pseudo second order model with a good compatibility between the experimental and theoretical Q_e values suggests that the adsorbant system in this study can be best described by the pseudo second order model. For the Weber Morris model of interparticular diffusion represented by the Eq. (10) and the Fig. S5, it is essential for the $q_t \sim t^{1/2}$ plot to go through the origin if the intraparticle diffusion is the sole rate-limiting step [48]. Therefore it can be concluded that the pseudo –second-order model gives a better fit than the two other models (pseudo-first-order and intraparticle diffusion models)

Table 4 Parameters of kinetic equations

Kinetic equations	Q_e (mg/g)	K_1 (min^{-1})	K_2 (g/mg min)	K_{ip} (min^{-1})	R^2
Psedo first order reaction	12.64	0.111			0.881
Pseudo second order reaction	51.02		0.0404		0.997
Interparticle diffusion model				1.5038	0.866

Q_e, K_1, K_2, K_{ip} and R^2 calculated from kinetic plots, Q_e (eperimental): 50.69

Table 5 Uranium conc.10 mg/L, pH 6, wt of ceria nanocrystals: 0.01 g, contact time: 1 h

Number of cycles	Uranium added (mg/L)	Adsorption (%)	Uranium leached (%)
First cycle	10	98.7	–
Second cycle	10	97.7	–
Third cycle	10	92.2	–
Fourth cycle	10	90.1	–
Fifth Cycle	10	88.0	97.6

Table 6 Effect of diverse anions and cations: pH 6, volume 500 mL, weight of ceria nanocrystal 0.05 g, time of contact 2 h

Cation/anion	Ion concentration in supernatant (mg/L)	
	Before adsorption	After adsorption
U	5	0.1
	5	0.5
	5	0.2
Na	75	72
	130	130
	10830	10800
K	4	4
	5	4
	345	343
Ca	85	70
	295	290
	500	495
Mg	35	30
	55	50
	1315	1280
Cl	160	155
	200	195
	31240	30400
SO_4^{2-}	60	55
	110	100
	2450	2440
F	0.4	0.4
	0.6	0.6
	0.5	0.5

suggesting that chemisorption may be partially contributing to the rate limiting step involving valency forces through sharing or exchange of electrons between sorbent and sorbate providing best correlation of the data [49].

Adsorption mechanism

The detailed study of the adsorption process of uranyl ions onto the ceria nanocrystal surface revealed that the mechanism is pH dependent and hence the adsorption mechanism was partially contributed to the electrostatic forces of attraction of the charged nanocrystal surface towards the neutral and the cationic uranyl species present in the aqueous medium at the specified pH. From the isothermal studies it could be concluded that the empirical values correlated well with Langmuir model of adsorption indicating monolayer coverage of the adsorbate on the adsorbent. The kinetic plot as depicted in Fig. 8 indicated an instant adsorption initially, followed by a steep rise in percent adsorption and then a gradual increase till the equilibrium was reached, which have been attributed to two mechanistic approaches. The reversible change in the oxidation state of cerium ions Ce(IV) to Ce(III) creating neutral surface/subsurface oxygen vacancies in ceria is a well established defect which increases with decrease in size and reducing atmosphere [13]. This has also been confirmed by the studies which show an increase in the concentration of Ce(III) as the crystallite size decreases [49] The rapid increase in adsorption at a very short time interval has also been contributed to the physisorption of uranyl ion into the surface oxygen vacancies and diffusion

Table 7 Application to real samples: pH 6, wt of ceria nanocrystal 0.05 g, contact time 20 h; volume of sample 500 mL

Cation/anion	Concentration in aq phase	AMD-1	AMD-2	AMD-3	AMD-4	AMD-5
U(μg/L)	Initial	160	338	247	138	200
	After adsorption	4	3	4	2	4
	Leaching with 5% NH_4HCO_3	151	330	241	129	195
Na(mg/L)	Initial	750	1111	1350	445	840
	After adsorption	748	1110	1344	440	840
K(mg/L)	Initial	30	5	3	3	4
	After adsorption	30	5	3	3	4
Ca(mg/L)	Initial	100	185	230	155	225
	After adsorption	85	172	221	140	200
Mg(mg/L)	Initial	75	200	210	85	295
	After adsorption	70	192	200	83	290
Cl(mg/L)	Initial	802	1995	1850	655	2080
	After adsorption	702	1900	1800	620	2000
SO_4^{2-}(mg/L)	Initial	612	1611	1350	400	630
	After adsorption	600	1600	1325	389	620
F^- (mg/L)	Initial	0.7	1.3	0.6	1.4	0.9
	After adsorption	0.7	1.3	0.6	1.4	0.9

into the non- uniformly formed nanopores within the ceria nanocrystal moiety. The stage of further gradual increase in adsorption is assumed to be controlled by intra-particle diffusion. This is also confirmed by the linear plot of Q_e vs. $t^{1/2}$ (Fig. S5). The intercept obtained by the extrapolation of the linear plot onto the Y-axis provided the measure of the boundary layer thickness which implies that there is some degree of boundary layer control between the aqueous medium, uranyl ions and the ceria surface active sorption sites. This boundary layer control is assumed to be related to the rate controlling mechanism and involves electrostatic interactions [49–51].

Reusability and recovery studies

In order to evaluate the further efficiency in application of the methodology to real samples the repeated practicability of the CeO_2 nanocrystals for U(VI) adsorption was also studied via many cycles of adsorption by repeated addition of 10 mg/L U(VI) through multiple cycles at the specified optimized parameters. This was followed by measurement of supernatant metal ion concentration by ICP-OES/LED. After each cycle the uranium concentration in the aqueous phase was monitored. After five such consecutive cycles the sum total of the uranium adsorbed on the nano adsorbent was quantitatively leached with 5% (w/v) ammonium bicarbonate and the desoprtion efficiency thus obtained was depicted in Table 5. After the cycles of adsorption–desorption the adsorbent was centrifuged and washed thoroughly with deionised water and ethanol to neutrality at room temperature and separated at a speed of 1500 rpm. Following which the adsorbent was dried under infrared lamp and thus reconditioned for adsorption in the succeeding cycles. Thus a satisfactory uranium recovery method after five cycles was obtained. The results of the above study also demonstrate that CeO_2 nanocrystals have a potential application prospect for preconcentration of U(VI) from large volumes of aqueous solutions in course of removal of uranium contamination.

Effect of diverse anions and cations

To study the effect of various cations and anions commonly occurring in major quantities in potable, effluent and marine water samples, the adsorption of U(VI) on ceria nanocrystals in presence of the cations like Na ($\sim$100–10,000 mg/L), K ($\sim$10–400 mg/L), Ca ($\sim$100–500 mg/L), Mg ($\sim$50–1500 mg/L), Cl ($\sim$150–30,000 mg/L), SO_4 ($\sim$50–2500 mg/L) and F ($\sim$0.5–1.0 mg/L) were studied as shown in Table 6 at the optimized parameters. The observations suggested a staggered adsorption of uranium in the real sample environment. This could not largely be attributed to competitiveness for the active sites of the adsorbent between the metal ion and the others as there was

no drastic difference in the concentrations of the other ions in the supernatant after adsorption equilibrium was reached. This proved the high selectivity of the adsorbent even when the ions were present in the ratio of 1:10,000.

Application to mine effluent samples

An attempt was made to apply the study to mine water samples received from exploratory mine areas of uranium. 500 mL of sample aliquot was taken with varying uranium concentrations. Experiments were conducted at pH 6 and a total contact time of 20 h including 4 h shaking on the magnetic stirrer. Uranium and other major anions and cations concentrations were monitored in the supernatant as tabulated in Table 7. As is depicted in this study ceria nanocrystals could be successfully used as an efficient selective adsorbent for removal of uranium contaminant which could be then be quantitatively recovered after leaching with 5% NH_4HCO_3. Hence this methodology can be further applied for preconcentration studies along with remediation on a larger scale.

Conclusion

The ceria nanocrystals were synthesized using a template free and ecofriendly methodology and were successfully applied for the selective adsorption of U(VI) ions from aqueous solutions at a near neutral pH. The experimentally observed adsorption results confirm the high efficiency of the nanosized material towards the remediation and preconcentration of the radionuclide in presence of varying aqueous environments through multicycles. The nanosized adsorbent by the virtue of its high surface area, mixed surface valency resulting in easily accessible oxygen vacancies and cavities of varying morphology and geometry in it's moiety, are very favorable for uranium adsorption. The experimental results in batch experiments were in good agreement with pseudo second order kinetic model [52]. The empirical data of the variation of concentration of the metal ion fitted better with Langmuir adsorption isotherm model when compared to the Freudlich model [53]. Hence the above methodology studied and optimized for uranium adsorption using ceria nanocrystals is economical, selective and environmentally benign. The study can be further scaled up for industrial/potable water remediation as well as preconcentration of the radionuclide from secondary sources of uranium like sea water.

work. The authors are also thankful to Regional Director and Deputy Regional Director, SR for their encouragement. The authors extend their thanks to Dr B.M. Reddy, IICT Hyderabad for providing the instrumental facilities for solid state characterization.

References

1. Lu Y, Chen W (2012) Sub-nanometre sized metal clusters: from synthetic challenges to the unique property discoveries. Chem Soc Rev 41:3594–3623
2. de Silva JMS, Strauss M, Maroneze CM, Souza ER, Gushikem Y, Sigoli FA, Mazali IO (2012) Size controlled synthesis of highly dispersed anatase/rutile nan oparticles with photocatalytic activity toward salicylic acid degradation. J Mater Chem 21:5390–5397
3. Cao CY, Qu J, Yan WS, Zhu JF, Wu ZY, Song WG (2012) Low-cost synthesis of flowerlike α-Fe$_2$O$_3$ nanostructures for heavy metal ion removal: adsorption property and mechanism. Langmuir 28:4573–4579
4. Hua M, Zhang S, Pan B, Zhang W, Zhang Q (2012) Heavy metal removal from water/wastewater by nanosized metal oxides: a review. J Hazard Mater 317:211–212
5. Shih JS, Wu YY, Chen CY, Yu CY (2012) Controlled morphological structure of ceria nanoparticles prepared by spray pyrolysis. Procedia Eng 36:186–194
6. Jieyun J, Tianqi L, Zhao L, Shirong L, Guolin H, Adesina AA (2017) Preparation of hollow SiO$_2$ microspheres functionalized with amidoxime groups for highly efficient adsorption of U(VI) from aqueous solution. J Radioanal Nucl Chem 311:2029–2037
7. Daqian L, Zhirong L, Changfu W, Yi L (2016) Removal of uranium(VI) from aqueous solution using nanoscale zero-valent iron supported on activated charcoal. J Radioanal Nucl Chem 310:1131–1137
8. Hongbin Z, Limin Z, Zhiwei H, Zhirong L, Taian L (2017) Characteristics of equilibrium and kinetic for U(VI) adsorption using novel diamine–functionalized hollow silica microspheres. J Radioanal Nucl Chem 311:269–278
9. Spendlikova I, Nemec M, Steier P, Keceli G (2017) Adsorption of uranium on freshly prepared hydrous titanium oxide and its utilization in determination of ^{236}U using accelerator mass spectrometry. J Radioanal Nucl Chem 311:447–453
10. Yanan W, Xia L, Yongshun H, Tasawar H, Ahmed A (2017) Interaction mechanisms of U(VI) and graphene oxide from the perspective of particle size distribution. J Radioanal Nucl Chem 311:209–217
11. Feng Q, Zhang Z, Ma Y, He X, Zhao Y, Chai Z (2012) Adsorption and desorption characteristics of arsenic onto ceria nanoparticles. Nanoscale Res Lett 7:84–91
12. Tsunekawa S, Ishikawa K, Kawazoe Y, Kasuya A (2000) Origin of anomalous lattice expansion in oxide nanoparticles. Phys Rev Lett 85:3440–3443
13. Kulgren J (2012) Oxygen vacancy chemistry in ceria. Uppsala University, Ph.D. thesis, Sweden
14. Sahu T, Bisht SS, Das KR, Kerkar S (2013) Nanoceria: synthesis and biomedical applications. Curr Nanosci 9:588–593
15. Peng XJ, Luan ZK, Ding J, Di ZH, Li Y, Tian BH (2005) Ceria Nano particles supported on carbon nanotubes for the removal of arsenate from water. Mater Lett 59:399–403
16. Di ZC, Ding J, Peng XJ, Li YH, Luan ZK, Liang J (2006) Chromium adsorption by aligned carbon nanotubes supported ceria nanoparticles. Chemosphere 62:861–865
17. Zhong LS, Hu JS, Cao AM, Liu Q, Song W, Wan G (2007) 3D flower like ceria/micro/nanocomposite structure and its

18. Hassan HS, El-Rehman KMA, El-Sayed AA (2011) Kinetic study of Zn^{2+} and Cd^{2+} ions adsorption by cerio oxide powder. Int J Environ Eng Sci 2:83–99
19. Reddy BM, Khan A (2005) Nanosized CeO$_2$–SiO$_2$, CeO$_2$–TiO$_2$, and CeO$_2$–ZrO$_2$ mixed oxides: influence of supporting oxide on thermal stability and oxygen storage properties of ceria. Catal Surv Asia 9:155–171
20. Sudarsanam P, Kuntaiah K, Reddy BM (2014) Promising ceria-samaria-based nanooxides for low temperature soot oxidation: a combined study of structure-activity properties. New J Chem 38:5991–6001
21. Cao CY, Cui ZM, Chen CQ, Song WG, Cai W (2010) Ceria hollow nanospheres produced by a template-free microwave-assisted hydrothermal method for heavy metal ion removal and catalysis. J Phys Chem C 114:9865–9870
22. Reddy BM, Katta L, Thrimurthulu G (2010) Novel nanocrystalline Ce$_{1-x}$La$_x$O$_{2-\delta}$ (x = 0.2) solid solutions: structural characteristics and catalytic performance. Chem Mater 22:467–475
23. Fangli F, Huanjie D, Jing B, Xiaolei W, FuanL Wei T, Yang W, Zhi Q (2011) Sorption of uranium(VI) from aqueous solution onto magnesium silicate hollow spheres. J Radioanal Nucl Chem 289:367–374
24. Exbrayat L, Steyer P, Rébéré C, Berziou C, Savall C, Ayrault P, Tertre E, Joly-Pottuz GL, Creus J (2014) Electrodeposition of zinc–ceria nanocomposite coatingsin alkaline bath. J Solid State Electrochem 18:223–233
25. Yudina T (2016) Synthesis, kinetic control and properties engineering of cerium oxide nanoparticles for biomedical applications. PhD thesis, Universitat Autonoma de Barcelona (UAB)
26. Liu X, Ray JR, Chelsea WN, Li Q, Jun YS (2010) Enhanced colloidal stability of CeO$_2$ nanoparticles by ferrous ions: adsorption, redox reaction, and surface precipitation. Environ Sci Technol 49:5476–5483
27. Patila S, Sandberg A, Heckert E, Self W, Seal S (2007) Protein adsorption and cellular uptake of cerium oxidenanoparticles as a function of zeta potential. Biomaterials 28:4600–4607
28. Krestou A, Panias D (2004) Uranium (VI) speciation diagrams in the UO$_2^{2+}$/CO$_3^{2-}$/H$_2$O system at 25 °C. Eur J Miner Process Environ Prot 4:113–129
29. Tripathi S, Bose R, Roy A, Nair S, Ravishankar N (2015) Synthesis of hollow nanotubes of Zn$_2$SiO$_4$ or SiO$_2$: mechanistic understanding and uranium adsorption behaviour. ACS Appl Mater Interfaces 7:26430–26436
30. Ishfaqa T, Naveed S, Kazmia M, Haq NB, Ferozea N (2013) A detailed investigation on engineering parameters for Cd(II) removal by ripped citrus paradisi pulp waste. J Chil Chem Soc 58:2172–2176
31. Goswamia A, Raulb PK, Purkaita MK (2012) Arsenic adsorption using copper (II) oxide nanoparticles. Chem Eng Res Des 90:1387–1396
32. Rezaei A, Hadi Khani H, Farahania MM, Rofouei MK (2012) A novel extraction and preconcentration of ultra-trace levels of uranium ions in natural water samples using functionalized magnetic-nanoparticles prior to their determination by inductively coupled plasma-optical emission spectrometry. Anal Methods 24:4107–4114
33. Baik MH, Hahn PS (2001) Experimental study on uranium sorption onto silica colloids: effects of geochemical parameters. J Korean Nucl Soc 33:261–269
34. Langmuir I (1918) The adsorption of gases on plane surfaces of glass, mica and platinum. J Am Chem Soc 40:1361–1403
35. Bird PG (1933) A derivation of Langmuir's adsorption isotherm. J Chem Educ 10:237

36. Hall KR, Eagleton LC, Acrivos A, Vermeulen T (1966) Pore and solid-diffusion kinetics in fixed bed adsorption under constant pattern conditions. Ind Eng Chem Fundam 5:212–223

37. Chowdhary ZZ, Zain SM, Khan RA, Khalid K (2011) Linear regression analysis for kinetics and isotherm studies of sorption f manganese (II) ions onto activated palm ash from waste water. Orient J Chem 27:405–415

38. Nilchi A, Dehaghan TS, Garmarodi SR (2013) Kinetics, isotherm and thermodynamics for uranium and thorium ions adsorption from aqueous solutions by crystalline tin oxide nanoparticles. Desalination 321:67–71

39. Guixia Z, Tao W, Xin Y, Shubin Y, Jiali L, Jun H, Dadong S, Xiangke W (2012) Preconcentration U(VI) ions on few-layered graphene oxide nanoshetts from aqueous solutions. Dalton Trans 41:6182–6188

40. BudnyakaTM Alexander VS, Agnieszka GP, Dariusz S, Igor VK, Dorota K, Marek M, Valentin A, Tertykhaa C (2016) Silica with immobilized phosphinic acid-derivative for uranium extraction. J Hazard Mater 314:326–340

41. Daqian L, Zhirong L, Changfu W, Yi L (2016) Removal of U(VI) from aqueous solutions using anano scale zero valent iron suppported on activated charcoal. J Radianal Nucl Chem 310:1131–1137

42. Cao Q, Huang F, Zhuang Z (2012) A study of the potential application of nano-Mg(OH)$_2$ in adsorbing low concentrations of uranyl tricarbonate from water. Nano scale 4:2423–2430

43. Young DM, Crowell AD (1962) Physical adsorption of gasses. Butterworth Ltd., London

44. Freundlich H (1925) The elements of colloidal chemistry. Butler & Tanner Ltd., London

45. Areco MM, Afonso MS (2010) Equilibrium and kinetics modeling biosorption of Zn(II) in aqueous solution using durian (Durio zibethinus) seed as low-cost biosorbent. Colloids Surf B 81:112–122

46. Dada AO, Olalekan A, Olatunya A, Dada O (2012) Langmuir, Freundlich, Temkin and Dubinin-Radushkevich isotherms studies of equilibrium sorption of Zn^{2+} unto phosphoric acid modified rice husk. J Appl Chem (IOSR-JAC) 3:38–45

47. Ho YS, McKay G (1999) Pseudo-second order model for sorption processes. Process Biochem 34:451–465

48. Hui Q, Lu LV, Pan BC, Zhang QJ, Zhang WM, Zhang QX (2009) Critical review in adsorption kinetic models. J Zhejiang Univ Sci A 10:716–724

49. Jose ML, Alexander LG, Tomás G, Benjamín S, Said A, Laura TM (2015) The prevalence of surface oxygen vacancies over the mobility of bulk oxygen in nanostructured ceria for the total toluene oxidation. Appl Catal B 174:403–412

50. Diagboya PN, Olu-Owolabi BI, Adebowale KO (2014) Microscale scavenging of pentachlorophenol in water using amine and tripolyphosphate-grafted SBA-15 silica: batch and modelling studies. J Environ Manag 146:42–49

51. Cheung WH, Szeto YS, McKay G (2007) Intraparticle diffusion processes during acid dye adsorption onto chitosan. Biores Technol 98:2897–2904

52. Gupta PC, Mallia MB, Das D, Suresh kumar MK (2010) Adsorption of uranium from aqueous solution using chitosan-tripolyphosphate (CTPP) beads. J Hazard Mater 184:65–72

53. Senthil PK, Kirthika K (2009) Equilibrium and kinetic study of adsorption of nickel from aqueous solution onto bael tree leaf powder. J Eng Sci Technol 4:351–363